

Modified viscosity in accretion disks. Application to Galactic black hole binaries, intermediate mass black holes and AGN

Mikołaj Grzędzielski¹, Agnieszka Janiuk¹, Bożena Czerny¹ and Qingwen Wu²

¹ Center for Theoretical Physics, Polish Academy of Sciences, Al. Lotników 32/46, 02-668 Warsaw, Poland
e-mail: mikolaj@cft.edu.pl

² School of Physics, Huazhong University of Science and Technology, Wuhan 430074, China

Received ...; accepted ...

ABSTRACT

Aims Black holes surrounded by accretion disks are present in the Universe in different scales of masses, from microquasars up to the Active Galactic Nuclei. Since the work of Shakura and Sunyaev (1973) and their α -disk model, various prescriptions for the heat production rate are used to describe the accretion process. The current picture remains still ad hoc, due the complexity of the magnetic field action. In addition, the accretion disks at high Eddington rates can be radiation-pressure dominated and, according to some of the heating prescriptions, thermally unstable. The observational verification of their resulting variability patterns may shed the light on both the role of radiation pressure and magnetic field in the accretion process.

Methods We compute the structure and time evolution of an accretion disk, using the code GLADIS (which models the Global Accretion Disk Instability). We supplement this model with a modified viscosity prescription, which can to some extent describe the magnetization of the disk. We study the results for a large grid of models, to cover the whole parameter space, and we derive conclusions separately for different scales of black hole masses, which are characteristic for various types of cosmic sources. We show the dependences between the flare, or outburst, duration, its amplitude and period, on the accretion rate and viscosity scaling.

Results We present the results for the three grids of models, designed for different black hole systems (X-ray binaries, intermediate mass black holes, and galaxy centers). We show that if the heating rate in the accretion disk grows more rapidly with the total pressure and temperature, the instability results in the longer, and sharper flares. In general, we find that the disks around the supermassive black holes are more radiation-pressure dominated and present relatively brighter bursts. Our method can also be used as an independent tool for the black hole mass determination, which we confront now for the intermediate black hole in the source HLX-1. For both the microquasars and Ultraluminous X-ray sources, we reproduce their observed lightcurves. We also compare the duration times of the model outbursts with the ages and bolometric luminosities of AGN.

Conclusions With our modeling, we justify the modified μ -prescription for the stress tensor $\tau_{r\phi}$ in the accretion flow in the microquasars. The discovery of the Ultraluminous X-ray source HLX-1, claimed to be an Intermediate Black Hole, gives further support to this result. The exact value of the μ parameter, as fitted to the observed lightcurves, may be treated as a proxy for the magnetic field strength in the accretion flow in particular sources, or their states.

Key words. black hole physics; accretion; viscosity

1. Introduction

Accretion disks are ubiquitous in the astrophysical black holes environment, and populate a large number of known sources. The black hole masses range from stellar mass black holes in X-ray binaries, through the intermediate mass black holes, up to the supermassive ones in quasars and active galaxy centers. The geometrically thin, optically thick accretion disk that is described by theory of Shakura and Sunyaev is probably most relevant for the high/soft spectral states of the black hole X-ray binaries, as well as for some active galaxies, e.g. the Narrow Line Seyfert 1 and numerous radio quiet quasars (Brandt et al. 1997; Peterson et al. 2000; Foschini et al. 2015). The basic theory of a geometrically thin, stationary accretion is based on the simple albeit powerful α prescription for the viscosity in the accreting plasma, introduced by Shakura & Sunyaev (1973). This simple scaling of the viscous stress with the pressure is also reproduced in the more recent numerical simulations of magnetized plasmas (Hirose et al. 2006; Jiang et al. 2013; Mishra et al. 2016). However, the latter are still not capable of modeling the global dynamics,

time variability and radiation emitted in the cosmic sources, and hence cannot be directly adopted to fit the observations.

The global models, however, must go beyond the stationary model, as the time-dependent effects connected with the non-stationary accretion are clearly important. In particular, a number of observational facts support the idea of a cyclic activity in the high accretion rate sources. One of the best studied examples is the microquasar GRS 1915+105, which in some spectral states exhibits cyclic outbursts of its X-ray luminosity, well fitted to the limit cycle oscillations of an accretion disk in the timescales of tens or hundreds of seconds Taam et al. (1997); Belloni et al. (2000); Neilsen et al. (2011). Those heartbeat states are known since 1997, when the first XTE PCA observations of this source were published (Taam et al. 1997), while recently yet another microquasar of that type, IGR J17091-3624, was discovered (Revnivtsev et al. 2003; Kuulkers et al. 2003; Capitanio et al. 2009), and the heartbeat states were also found for this source (Altamirano et al. 2011b; Capitanio et al. 2012; Pahari et al. 2014; Janiuk et al. 2015). Furthermore, a sample of sources proposed in Janiuk & Czerny (2011) was suggested to undergo

luminosity oscillations, possibly induced by the non-linear dynamics of the emitting gas. This suggestion was confirmed by the recurrence analysis of the observed time series, presented in Suková et al. (2016).

One of the possibilities to drive the non-linear process in the accretion disk is its thermal and viscous oscillation induced by the radiation pressure term. It can be dominant for high enough accretion rates in the innermost regions of the accretion disk, which are the hottest. The timescales of such oscillations depend on the black hole mass, and for the stellar mass BH systems are on the order of tens to hundreds of seconds. For a typical supermassive black hole of $10^8 M_\odot$, the process would require timescales of hundreds of years. Therefore, in AGN we cannot observe the evolution under the radiation pressure instability directly. Nevertheless, statistical studies may shed some light on the sources evolution. For instance, the Giga-Hertz Peaked quasars (Czerny et al. 2009) have very compact sizes which would directly imply their ages. In case of a limit-cycle kind of evolution, in fact these sources would not be very young, but 'reactivated'. Another observational hint is the shape of distortions or discontinuities in the radio structures. These structures may reflect the history of the central power source of a quasar, which went through the subsequent phases of activity and quiescence. An exemplary source of that kind, quasar FIRST J164311.3+315618, was studied in Kunert-Bajraszewska & Janiuk (2011), and found to exhibit multiple radio structures. Another class of objects which are claimed to contain the BH accretion disk are the Ultraluminous X-ray sources (ULXs). ULXs are the class of sources having the luminosity larger than the Eddington one for the heaviest stellar-mass objects ($> 10^{40}$ ergs s^{-1}). Therefore, ULXs are frequently claimed to contain accreting black holes with masses larger than the most massive stars and lower than the AGNs ($10^3 - 10^6 M_\odot$). An example object in this class is HLX-1, which is possibly the best known candidate for an intermediate mass black hole (Lasota et al. 2011). The source is located near the spiral galaxy ESO 243-49 (Wiersema et al. 2010). Its peak luminosity exceeds 10^{42} erg s^{-1} . HLX-1 exhibits periodic limit-cycle oscillations. During seven years of observations of its X-Ray variability, six significant bursts lasting few tens of days have been noticed. The mass of the black hole inside HLX-1 is estimated at the level about $10^4 - 10^5 M_\odot$ (Straub et al. 2014). In this work, we investigate broad range of theoretical models of the radiation pressure driven outbursts and prepare the results for the easy confrontation with observational data. The appearance of the radiation pressure instability in hot parts of accretion disks can lead to significant outburst for all scales of the black hole mass. Temperature and heat production rate determine the outburst frequency and shape. Different effective prescriptions for turbulent viscosity affect the instability range and the outburst properties. Thus, by confronting the model predictions with observed outbursts, we can put the constraints on those built-in assumptions.

2. Model

2.1. Radiation pressure instability

In the α -model of the accretion disk, the non-zero component $\tau_{r\phi}$ of the stress tensor is assumed to be proportional to the total pressure. The latter includes the radiation pressure component, which scales with temperature as T^4 and blows up in hot, optically thick disks for large accretion rates. In general, adopted assumption about the dependence of the $\tau_{r\phi}$ on the local disk properties leads to the specific prediction of the behavior of the

disk heating. This in turn affects the heating and cooling balance between the energy dissipation and radiative losses.

Such a balance, under the assumption of hydrostatic equilibrium, is calculated numerically with a closing equation for the locally dissipated flux of energy given by the black hole mass and global accretion rate. The local solutions of the thermal balance and structure of the stationary accretion disk at a given radius may be conveniently plotted in the form of the so-called stability curve of the shape S . Here, distinct points represent the annulus in a disk, with temperature and surface density determined by the accretion rate. For small accretion rates, the disk is gas pressure dominated and stable. The larger the global accretion rate, the more annuli of the disk will be affected by the radiation pressure and the extension of the instability zone grows in radius. The hottest area of the disk are heated rapidly, the density is decreasing and the local accretion rate is growing. More material is transported inwards. The disk annulus empties because of both increasing accretion rate and decreasing density, so there is no self-regulation of the disk structure. However, the so called 'slim-disk' solution (Abramowicz et al. 1988), where the advection of energy provides additional source of cooling in the highest accretion rate regime (close to the Eddington limit), provides a stabilizing branch. Hence, the advection of some part of energy allows the disk to survive and oscillate between the hot and cold states. Such oscillating behavior leads to periodic changes of the disk luminosity. To model such oscillations, obviously, the time-dependent structure of the accretion flow needs to be computed, instead of the stationary solutions, described by the S -curve.

2.2. Equations

We are solving the time-dependent vertically averaged disk equations with radiation pressure in the Newtonian approximation, following the methods described in Janiuk et al. (2002), and subsequent papers (Janiuk & Czerny 2005; Czerny et al. 2009; Janiuk et al. 2015). The disk is rotating around the central object with mass M with Keplerian angular velocity $\Omega = \sqrt{\frac{GM}{r^3}}$, and maintains the local hydrostatic equilibrium in the vertical direction $P = C_3 \Sigma \Omega^2 H$. The latter gives the necessary relationship between pressure P , angular velocity Ω and disk vertical thickness H . C_3 is the correction factor regarding the vertical structure of the disk. In our model $C_3 = \frac{\int_0^H dz P(z)}{P(z=0)H}$. The vertically averaged stationary model is described in the paper (Janiuk et al. 2002). In the stationary (initial condition) solution, the disk is emitting the radiation flux proportional to the accretion rate, \dot{M} , fixed by the mass and energy conservation laws

$$F_{\text{tot}} = Q_+ = \frac{3GM\dot{M}}{8\pi r^3} f(r), \quad (1)$$

where $f(r) = 1 - \sqrt{r_{in}/r}$ is the inner boundary condition term. In time-dependent solution the accretion rate is a function of radius, and assumed accretion rate at the outer disk radius forms a boundary condition. We solve two partial differential equations describing the viscous and thermal evolution of the disk:

$$\frac{\partial \Xi}{\partial t} = \frac{12}{y^2} \frac{\partial^2}{\partial y^2} (\Xi \nu), \quad (2)$$

where $y = 2r^{1/2}$ and $\Xi = 2r^{1/2}\Sigma$, and

$$\frac{\partial \ln T}{\partial t} + \nu_r \frac{\partial \ln T}{\partial r} = q_{\text{adv}} + \frac{Q_+ - Q_-}{(12 - 10.5\beta)PH}. \quad (3)$$

The first equation represents the thin accretion disk's mass diffusion, and the second equation is the energy conservation. Here ν is the effective kinematic viscosity coefficient, which for thin disk geometry is connected with the heat production rate as follows:

$$\nu = \frac{Q_+}{\Sigma \Omega^2}. \quad (4)$$

Thus, calculation of ν requires the assumption about the heating term. The radial velocity in the flow is given by:

$$v_r = -\frac{3}{\Sigma} r^{-1/2} \frac{\partial}{\partial r} (\nu \Sigma r^{1/2}). \quad (5)$$

The quantity β is the ratio between gas and total (gas and radiation) pressure $\beta = \frac{P_{\text{gas}}}{P}$. The advection term,

$$q_{\text{adv}} = \frac{4 - 3\beta}{12 - 10.5\beta} \left(\frac{d \ln \rho}{dt} + v_r \frac{d \ln \Sigma}{dr} \right), \quad (6)$$

is computed through the radial derivatives. For the initial condition q_{adv} is taken to be a constant, of order of unity. The vertically averaged heating rate is given by:

$$Q_+ = C_1 \tau_{r\phi} r \frac{\partial \Omega}{\partial r} H, \quad (7)$$

where $\tau_{r\phi}$ is vertically averaged stress tensor:

$$\tau_{r\phi} = \frac{1}{2H} \int_{-H}^H dz T_{r\phi}, \quad (8)$$

and the radiative cooling rate per unit time per surface unit is

$$Q_- = C_2 \frac{4\sigma_B T^4}{3\kappa \Sigma}. \quad (9)$$

where κ is the electron scattering opacity, equal to $0.34 \text{ cm}^{-2} \text{ g}^{-1}$. Coefficient C_1 and C_2 in Eqs. (7) and (9) are derived from the averaged stationary disk model (Janiuk et al. 2002) and are equal to: $C_1 = \frac{\int_{-H}^H dz \rho(z)}{\rho(z=0)H} = 1.25$, $C_2 = 6.25$ respectively.

2.3. Expression for stress tensor - different prescriptions

The difficulty in finding the proper physical description of the turbulent behaviour of gas in ionized area of an accretion disk led to adoption of several distinct theoretical prescriptions of the non-diagonal stress tensor term $\tau_{r\phi}$. Gas ionisation should lead to existence of magnetic field created by the moving electrons and ions. The magnetic field in disk is turbulent and remains in thermodynamical equilibrium with the gas in disk. For proper description of the disk viscosity, different complex phenomena should be included in $\tau_{r\phi}$. For purely turbulent plasma we can expect the proportionality between the density of kinetic energy of the gas particles and energy of the magnetic field (Shakura & Sunyaev 1973). However, the disk geometry allows the magnetic field energy to escape (Sakimoto & Coroniti 1989; Nayakshin et al. 2000). Following Shakura & Sunyaev (1973), one can therefore assume the non-diagonal terms in the stress tensor proportional to the total pressure with a constant viscosity α :

$$\tau_{r\phi} = \alpha P. \quad (10)$$

On the other hand, Lightman & Eardley (1974) proved instability of the model described by Shakura & Sunyaev (1973).

Following that work, Sakimoto & Coroniti (1981) proposed another formula which led to a set of stable solutions without any appearance of the radiation pressure instability:

$$\tau_{r\phi} = \alpha P_{\text{gas}}. \quad (11)$$

Later, Merloni and Nayakshin (Merloni & Nayakshin 2006), motivated by the heartbeat states of GRS 1915+105, investigated the square-root formula

$$\tau_{r\phi} = \alpha \sqrt{P P_{\text{gas}}}. \quad (12)$$

This prescription was introduced by Taam & Lin (1984) in the context of the Rapid Burster and used later by Done & Davis (2008) and Czerny et al. (2009) both for galactic sources and AGN.

In the current work, we apply a more general approach and introduce the entire family of models, with the contribution of the radiation pressure to the stress tensor parametrized by a power-law relation with an index $\mu \in [0, 1]$. We therefore construct a continuous transition between the disk which is totally gas pressure dominated and that with the radiation pressure that influences the heat production (Szuszkiewicz 1990; Honma et al. 1991; Watarai & Mineshige 2003; Merloni & Nayakshin 2006). The formula for the stress tensor is a generalization of the formulae those in Equations 10, 11, 12) and is given by:

$$\tau_{r\phi} = \alpha P^{\mu} P_{\text{gas}}^{1-\mu}. \quad (13)$$

In this work, we investigate the behaviour of the accretion disk described by formula (13) for a very broad range of black holes and different values of μ . Similar analysis has been performed also by Merloni & Nayakshin (2006) for different values of α (here, we fix our α with a constant value, which is at the level of 0.02). Regarding the existence of magnetic field inside the accretion disk, the viscosity can be magnetic in origin, and can reach different values for differently magnetized disks. As the strong global magnetic field can stabilize the disk (Czerny et al. 2003; Sadowski 2016), the parameter μ can be treated as an effective prescription of magnetic field.

2.4. Numerics

We use the code *GLADIS* (for the GLobal Accretion Disk InStability), which basic framework was initially described by Janiuk et al. (2002). The code was subsequently developed and applied in a number of works to model the evolution of accretion disks in Galactic X-ray binaries and AGN (Janiuk & Czerny 2005; Czerny et al. 2009; Janiuk & Misra 2012). The code allows for computations with a variable time-step down to a thermal timescale, adjusting to the speed of local changes of the disk structure. Our method was recently used for modeling the behaviour of the microquasar IGR J17091 (Janiuk et al. 2015). In that work, we used the prescription for a radiation-pressure dominated disk (with $\mu = 1$, explicitly), but with an explicit formula approximating wind outflow which regulates the amplitudes of the flares, or even temporarily leads to the completely stable disk. Here, we modified the methodology, and added the parameter μ , which allows for a continuous transition between the gas and radiation pressure dominated cases, e.g. with $\mu \in [0, 1]$, as described by the Equation 13. We neglect the wind outflow, though, as in many sources the observable constraints for its presence are too weak.

| Value | Symbol |
|----------------------------|-----------|
| Black hole mass | M |
| Accretion rate | \dot{m} |
| First viscosity parameter | α |
| Second viscosity parameter | μ |

Table 1. Summary of the model input parameters

| Value | Symbol |
|-----------------------------------|----------|
| Bolometric luminosity | L |
| Period | P |
| Amplitude (L_{\max}/L_{\min}) | A |
| Flare duration to period ratio | Δ |

Table 2. Summary of the characteristic quantities used to describe the accretion disk flares

2.5. Parameters and characteristics of the results

We start time-dependent computations from certain initial state, and evolve it for some time till the disk develops a specific regular behaviour pattern. We can get either a constant luminosity of the disk (i.e. stable solution), flickering, or the periodic lightcurves, depending on the model parameters. We parameterize the models by the global parameters: the black hole mass M , the external accretion rate, as well as the physical prescription for the stress, α and μ). In this study we limited our modeling to a constant (arbitrary) value of $\alpha = 0.02$, since the scaling with α is relatively simple.

Those parameters are not directly measured for the observed sources. In the current work, we focus on the unstable accretion disks. We thus construct from our models a set of output parameters which can be relatively easily measured from the observational data: the average bolometric luminosity L , the maximum bolometric luminosity L_{\max} , the minimum bolometric luminosity L_{\min} , the relative amplitude of a flare, $A = \frac{L_{\max}}{L_{\min}}$, and the period, P .

In order to parametrize shape of the lightcurve, we introduce also a dimensionless parameter Δ , which is equal to the ratio of the flare duration to the period. As a flare duration we define the time between moment with luminosity equal to $(L_{\max} + L_{\min})/2$ on the ascending slope of the flare, and the luminosity $(L_{\max} + L_{\min})/2$ on the descending slope of the flare. We then compare L , A , P and Δ obtained for several distinct black hole mass scales. In Table 1 we summarize the model input parameters. In Table 2 we summarize the probed characteristics of the resulting flares.

3. Local stability analysis

We first perform a local stability analysis in order to formulate basic expectations and limit the parameter space. In general, the disk is locally thermally unstable if for some temperature T and radius r , the local heating rate grows with the temperature faster than the local cooling rate:

$$\frac{d \log Q_+}{d \log T} > \frac{d \log Q_-}{d \log T}. \quad (14)$$

In this analysis, we consider the timescales that are different for the thermal and viscous phenomena which is justified for a thin disks.

3.1. Stability and timescales

For thin, opaque accretion disks, we have strong timescale separation between thermal (connected with the local heating and cooling), and viscous phenomena. The thermal timescale, for disk rotating with the angular velocity Ω , is $t_{\text{th}} = \alpha^{-1} \Omega^{-1}$. The appearance of viscous phenomena, connected with the large-scale angular momentum transfer is connected with the disk thickness, so that $t_{\text{visc}} = t_{\text{th}} \frac{R^2}{H^2}$. We focus now on the thermal phenomena. In thermal timescale the local disk surface density is constant, and only the vertical inflation is allowed, so for that timescale we can assume $\Sigma = \text{const}$. From Eqs. (7) and (12) we have:

$$Q_+ = \frac{3}{2} C_1 \alpha P^{\mu} P_{\text{gas}}^{1-\mu} H \Omega. \quad (15)$$

Assuming that the disk maintains the vertical hydrostatic equilibrium $H = P/(C_3 \Sigma \Omega)$, and defining $x = \frac{P_{\text{gas}}}{P_{\text{rad}}} + 0.5$, we can rewrite Eq. (15) as:

$$Q_+ = \frac{3}{2C_3 \Sigma \Omega} P^{1+\mu} P_{\text{gas}}^{1-\mu} = \frac{3}{2C_3 \Sigma \Omega} P_{\text{rad}} (x + 1/2)^{1+\mu} (x - 1/2)^{1-\mu}. \quad (16)$$

Then, if we assume a constant Σ regime, we have:

$$\frac{dx}{dT} = -\frac{7}{2} \frac{(x + 1/2)(x - 1/2)}{2xT} \quad (17)$$

and

$$\frac{d \log Q_+}{d \log T} = 1 + 7\mu \frac{1 - \beta}{1 + \beta} \quad (18)$$

where $\beta = \frac{P_{\text{gas}}}{P_{\text{tot}}} = \frac{x-1/2}{x+1/2}$. Finally, from Eq. (9) and Eq. (14), we have:

$$\frac{d \log Q_+}{d \log T} > 4, \quad (19)$$

which is fulfilled if the condition:

$$\beta < \frac{7\mu - 3}{7\mu + 3} \quad (20)$$

is satisfied (Szuszkiewicz 1990). This gives the necessary condition for the instability for the case of μ -model, so that the instability occurs only if $\mu > 3/7$.

3.2. Magnetized disk and its equivalence to μ model

Existence of strong magnetic fields can stabilize the radiation-pressure dominated disk (Svensson & Zdziarski 1994; Czerny et al. 2003; Sadowski 2016). We can assume a significant magnetic contribution to the total pressure P , defining it as follows:

$$P = P_{\text{rad}} + P_{\text{gas}} + P_{\text{mag}}. \quad (21)$$

Let us define the disk magnetization coefficient $\beta' = \frac{P_{\text{mag}}}{P_{\text{tot}}}$. We put the formula (21) into the Shakura-Sunyaev stress-energy tensor (i.e., for $\mu = 0$ in Eq. 16), and then we get:

$$\frac{d \log Q_+}{d \log T} = 8(1 - \beta'). \quad (22)$$

Here, the value of $\beta' = \frac{1}{2}$ means that there is an equipartition between the energy density of the gas-radiation and magnetic

energy density. It corresponds to the complete stabilization of the disk, so that $\frac{d \log Q_\perp}{d \log T} \leq \frac{d \log Q_\perp}{d \log T}$. From the formula (20) we can connect β' and μ as follows:

$$\mu = 1 - \frac{8}{7}\beta'. \quad (23)$$

Regarding the observed features, the model of magnetized disk is equivalent to the μ model for the radiation pressure dominated disks in terms of appearance of thermal instability. The major difference is that the greater total pressure makes the disk thicker. This fact can have some influence on the behaviour of the lightcurve, which we discuss below.

3.3. Disk magnetization and amplitude

The energy equation (3) can give us a direct connection between the heating rate and pressure. If we assume that the heating rate dominates the cooling rate, we have:

$$\frac{dT}{dt} = CT^{\gamma\mu-7}, \quad (24)$$

where C is a constant in the thermal timescale and depends on the local values of Σ and Ω . This simple, first order differential equation gives us the following dependence on the heating growth:

$$\frac{d \log T}{d \log t} = \frac{1}{7(1-\mu)}. \quad (25)$$

It explains why for bigger μ the outbursts are more sharp. It can also give another criterion for determination of a proper value of μ , and can be used as a test for the validity of μ -model in confrontation with the observational data. If we assume that most of the luminosity comes from a hot, thermally unstable region of the disk (Janiuk et al. 2015) and we apply it to (25), we get:

$$\frac{d \log L}{d \log t} = \frac{4}{7(1-\mu)}. \quad (26)$$

Regarding the timescale separation, and assuming that the flaring of the disk is stopped by the viscous phenomena after $t \approx t_{\text{visc}}$, we get the following formula for the dependence between the relative amplitude $A = \frac{L_{\text{max}}}{L_{\text{min}}}$ and the viscous to thermal timescales rate:

$$\log A = \frac{4}{7} \frac{1}{1-\mu} \log\left(\frac{t_{\text{visc}}}{t_{\text{th}}}\right). \quad (27)$$

Furthermore, we can derive a useful formula that connects the presence of magnetic fields with the amplitude of the limit-cycle oscillations:

$$\log A = \frac{1}{2} \frac{1}{\beta'} \log\left(\frac{t_{\text{visc}}}{t_{\text{th}}}\right). \quad (28)$$

In the rest of this article, we perform a more detailed analysis of the relation between the outburst amplitude and other lightcurve properties on the μ parameter, which is possibly corresponding to the scale of magnetic fields.

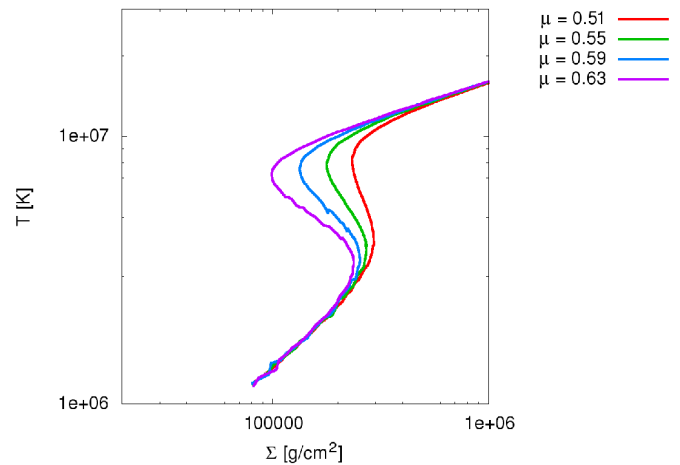


Fig. 1. Local stability curves for $\mu = 0.51$, $\mu = 0.55$, $\mu = 0.59$ and $\mu = 0.63$. Parameters: $M = 3 \times 10^4 M_\odot$, $\alpha = 0.02$, and $\dot{m} = 0.7$. The chosen radius is $R = 7.82R_{\text{Schw}} = 15.74 \frac{GM}{c^2} = 6.88 \times 10^{10} \text{ cm}$, corresponding to the inner, hot area of the disk. The curves depend strongly on the μ parameter, and larger μ provides larger negative derivative range corresponding to the unstable state.

4. Results - stationary model

First, we compute an exemplary set of stationary models, to verify the expected parameter range of the instability. Eq. (20) gives the relation between the maximum gas-to-total pressure ratio and minimum value of the μ parameter. We perform numerical computations for an intermediate black hole mass of $3 \times 10^4 M_\odot$, and plot the stability curve at the radius $R = 7.82R_{\text{Schw}} = 15.74 \frac{GM}{c^2} = 6.88 \times 10^{10} \text{ cm}$. The disk is locally unstable if the slope $\frac{\partial \Sigma}{\partial T}$ is negative (Eq. (14)). It gives the necessary, but not the sufficient condition for the global instability, as for the appearance of the significant flares, the area of the instability should be sufficiently large. We compute the S-curves (see Section 1), which are presented in the Figure 1 for different values of μ . The bigger μ , the bigger is the negative slope area on the S-curve, so that the larger range of the instability. However, only hot, radiation-pressure-dominated area of the disk remains unstable, and for larger radii the S-curve bend moves towards the enormously large, unphysical external accretion rate. In effect, for sufficiently large radii, the disk remains stable. The same trend is valid also for stellar mass (microquasars) and supermassive (AGN) black holes (Janiuk & Czerny 2011).

5. Results - time dependent model

In this section, we focus on the numerical computations of the full time-dependent model. We perform the full computations of the radiation pressure instability models since the stability curves give us only the information about the local disk stability. However, the viscous transport (Eq.(2)) and the radial temperature gradients deforms the local disk structure, and the time evolution of the disk at a fixed radius resulting from the global simulations does not necessarily follow the expectations based on local stability analysis.

In Figures 2 and 3 are presented the stability curves (red) and the global solutions of dynamical model plotted at the same single radius (green). Stronger bending of the shape of the lightcurves appearing for larger μ (Figs. 1, 2, and 3) affects in broader developing of the instability, visible in the shape of

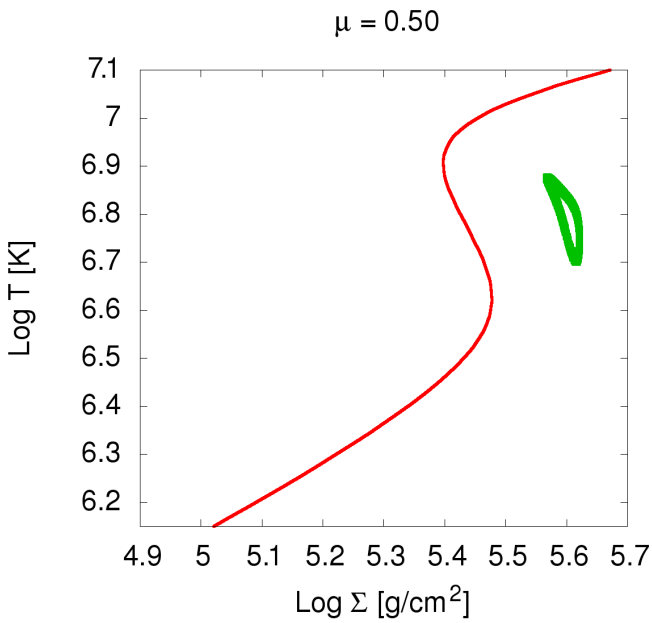


Fig. 2. T and Σ variability for the model with $\mu = 0.5$ with a typical ULX black hole mass. The computation shows a weakly developed instability. Parameters: $M = 3 \times 10^4 M_\odot$, $\alpha = 0.02$, and $\dot{m} = 0.25$. The plot is made for the radius $R = 7.82R_{Schw} = 15.74 \frac{GM}{c^2} = 6.88 \times 10^{10} \text{ cm}$. The red curve represents the stationary model and the green dots show local values of the temperature for the time-dependent computation.

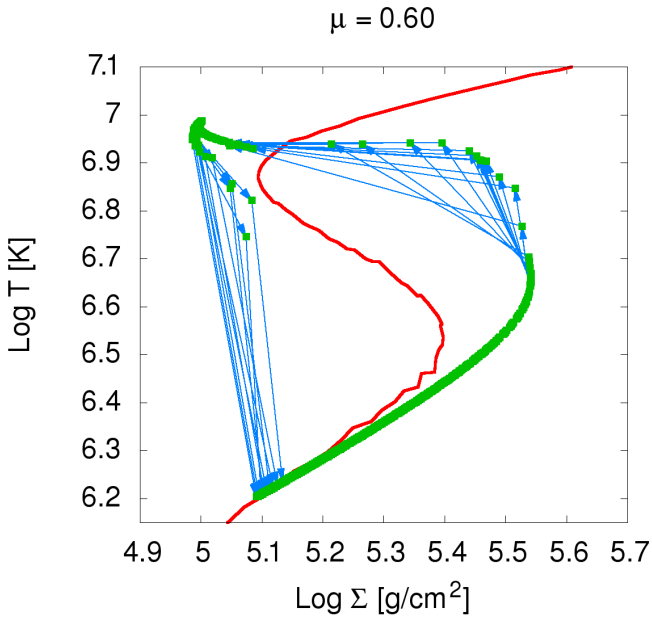


Fig. 3. T and Σ variability for model with $\mu = 0.6$ for a typical ULX black hole mass. The models presents a strongly developed instability, leading to huge outbursts. Parameters: $M = 3 \times 10^4 M_\odot$, $\alpha = 0.02$, and $\dot{m} = 0.25$ for the radius $R = 7.82R_{Schw} = 15.74 \frac{GM}{c^2} = 6.88 \times 10^{10} \text{ cm}$. The red curve represents the stationary solution and the green dots show local values of the temperature and density in the dynamical model. The points occupy both the upper and lower branches of the S-curve. Green points represent most common states of the disk, blue vectors - directions of the most common rapid changes of local T and Σ .

lightcurves (Figs. 4,5). Low value of μ causes the presence of the instability in a small range of radii so the instability is additionally dumped by the stable zones. The time-dependent solution never sets on the stability curve, the covered area in Fig.2 is very small, and the corresponding global lightcurve shows only small flickering. The growth of the instability for a large μ results in the dynamical values of T to form two coherent sets (see Figure 3), and the solution follows the lower branch of the stability curve. This part of the evolution describes the prolonged period between the outbursts.

For the comparison with the observed data we need to know the global time behaviour of the disk for a broad parameter range. We run grid of models for typical stellar mass $M = 10M_\odot$, for intermediate black hole mass $M = 3 \times 10^4 M_\odot$, and for supermassive black hole. We adopted $\alpha = 0.02$ throughout all the computations, and accretion rates ranged between $10^{-1.6}$ and $10^{-0.2}$ in Eddington units. For each mass, we present the relations between period, amplitude and duration divided by period. According to Czerny et al. (2009), the threshold accretion rate is (the sufficient rate for the outbursts to appear) is at the level of 0.025 for Active Galactic Nuclei. For our models, the critical value of accretion rate is at the level of $0.025 - 0.1$ of the Eddington rate. Below, we present our results through a set of mutual correlations between observable characteristics of the flares, P , A , and Δ (see Table 1), and the model parameters, \dot{m} , M and μ .

5.1. Lightcurves shape

We define here different characteristic modes of the outbursts. Since we have a dynamical system described by set of non-linear partial differential equations, we expect that the outbursts will form different patterns of variability, which should be comparable to the observed patterns. For that non-linear system we can distinguish between the flickering behaviour and the strong flares. In the Figures 4, and 5, we present the typical cases of flickering and outburst flares. The difference between the flickering and outburst modes lies not only in their amplitudes. As we can see in Figure 5, the long low luminosity phase, when the inner disk area remains cool, is not present in the flickering case, presented on Fig. 4. The latter, corresponds to the temperature and density variations presented in Fig. 2, where the surface density of the disk is not changing significantly. In contrast, Fig. 5 presents the case, when the surface density changes significantly and Σ needs a long time to grow to the value when the rapid heating is possible. In case of flickering we can distinguish two phases of the cycle: (i) heating, when the temperature in the inner regions of the disk is growing rapidly, and (ii) advective, when the inner annuli cool down significantly, and then extinct when disk is sufficiently cool. Now, after strong decrease of advection, the heating phase repeats again. In case of the burst, the phases (i) and (ii) are much more developed and advection is able to achieve instantenous thermal equilibrium of the disk, in contradiction to flickering, where disk is always unstable. The instantenous equilibrium leads to the third phase (iii), diffusive, when the surface density in the inner annuli of the disk is growing up to the moment when the stability curve has a negative slope, and the cooling rate, Q_- , is significantly smaller in comparison to the heating rate, Q_+ . Then, the phase of heating repeats.

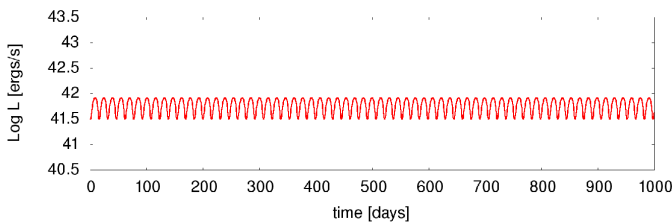


Fig. 4. Typical flickering lightcurve for intermediate mass black hole and smaller μ ($M = 3 \times 10^4$, $\mu = 0.5$ $\dot{m} = 0.25$)

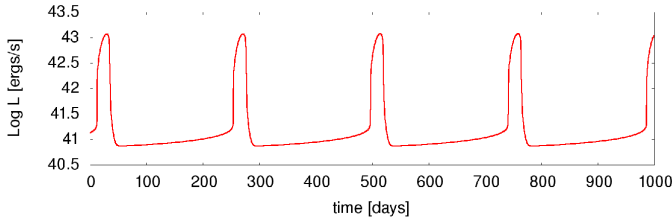


Fig. 5. Typical outburst lightcurve for intermediate mass black hole and larger μ ($M = 3 \times 10^4$, $\mu = 0.6$ $\dot{m} = 0.25$)

5.2. Amplitude maps

Figures 6, 7, and 8 show dependences between the accretion rate, μ coefficient, and outbursts' amplitude. The black area corresponds to cases of stable solutions without periodic outbursts. Violet area corresponds to a small flickering, and red and yellow areas correspond to bright flares. Since for a given accretion rate and μ the AGN disks are much more radiation-pressure dominated, the critical values of the accretion rates in Eddington units are the lowest for AGN. Thus, the stabilizing influence of magnetic field is more pronounced for the microquasars, than for AGN. Our results include different variability patterns. As shown in Figures 6, 7, and 8, for a given set of μ and accretion rate, the relative amplitude vary by many orders of magnitude (from small flares, changing the luminosity by only a few percent, up to the large outbursts with amplitudes of ~ 200 for microquasars, ~ 1000 for intermediate black holes, and ~ 2000 for AGN). The outbursts' amplitude grows with accretion rate and with μ . To preserve the average luminosity on sub-Eddington level, also the lightcurve shape should change with at least one of these parameters. Let Δ be flare duration to period ratio, as defined in Section 1. To preserve the average luminosity L , the energy emitted during the flare plus energy emitted during quiescence (between the flares) should be lower than the energy emitted during one period. Since the radiation pressure instability reaches only the inner parts of the disk, the outer stable parts of the disk radiate during the entire cycle, maintaining the luminosity at the level of L_{\min} . This level can be computed from the Eq. (1) since the outer border of the instability zone is known (Janiuk & Czerny 2011; Janiuk et al. 2015). Then Δ must satisfy the following relation:

$$\frac{1}{2}(L_{\min} + L_{\max})\Delta < L, \quad (29)$$

which means that there is a limit of:

$$\Delta < \frac{2(L/L_{\min})}{A + 1}. \quad (30)$$

This limitation can be seen in the Figures 15, 16 and 17.

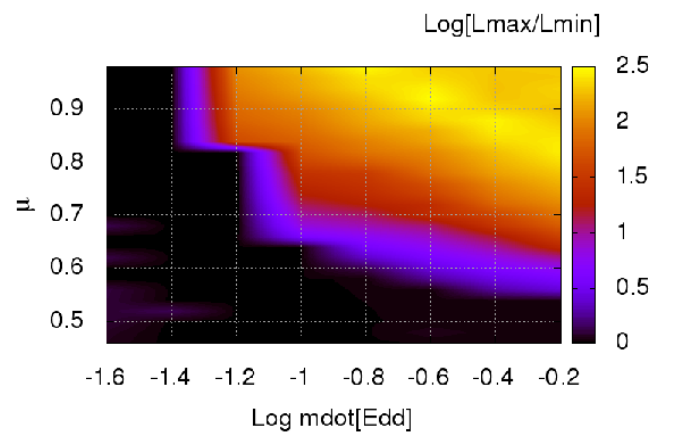


Fig. 6. Amplitude map for different values of accretion rates and μ for the accretion disk around a stellar mass black hole ($M = 10M_{\odot}$). Black region represents no flares and lack of the instability.

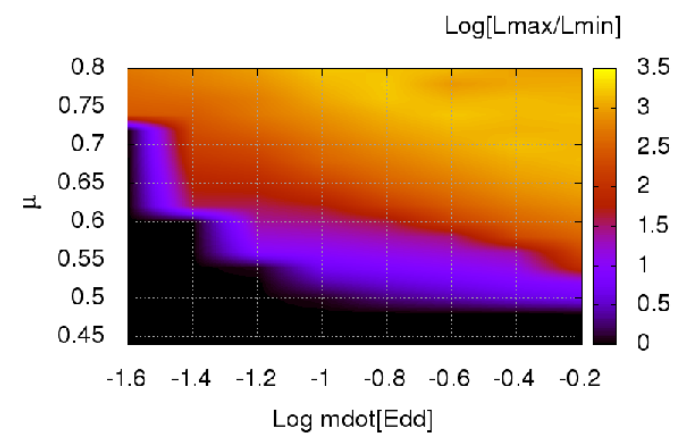


Fig. 7. Amplitude map for different values of accretion rates and μ for the accretion disk around an intermediate mass black hole ($M = 3 \times 10^4 M_{\odot}$). Black region represents no flares and lack of the instability.

5.3. Amplitude and period

In Figures 9, 10, and 11, we present the dependence between period and amplitude for the microquasars, intermediate mass black holes and AGN, respectively. In general, the amplitude grows with the period P , μ , and accretion rate \dot{m} . The results shown by points in Figures 9, 10, and 11, can be fitted with the following formula:

$$\log P [\text{sec}] \approx 0.83 \log \frac{L_{\max}}{L_{\min}} + 1.15 \log M + 0.40. \quad (31)$$

Here P is the period in seconds and M is the mass in Solar masses. The above general relation gains the following forms, if we want to use it in the application for the sources with different black hole mass scales:

$$\log P_{\text{MICR}} [\text{sec}] \approx 0.83 \log \frac{L_{\max}}{L_{\min}} + 1.15 \log \frac{M}{10M_{\odot}} + 1.55, \quad (32)$$

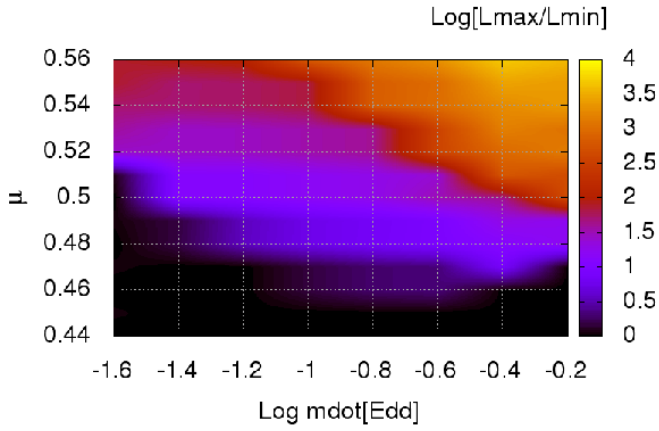


Fig. 8. Amplitude map for different values of accretion rates and μ for the accretion disk around a supermassive black hole ($M = 10^8 M_\odot$). Black region represents no flares and lack of the instability.

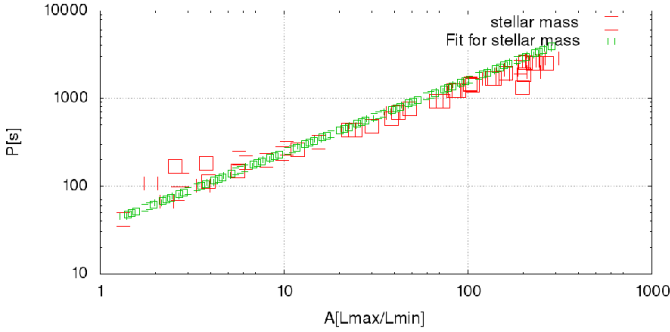


Fig. 9. Dependence between period and amplitude of outbursts for a stellar mass black hole ($M = 10 M_\odot$). The graph was prepared for a range of $\mu \in [0.44 : 0.8]$.

for the microquasars (see fit on Fig. 9), then

$$\log P_{\text{IMBH}} [\text{days}] \approx 0.83 \log \frac{L_{\text{max}}}{L_{\text{min}}} + 1.15 \log \frac{M}{3 \times 10^4 M_\odot} + 0.53 \quad (33)$$

for intermediate mass black holes (see fit on Fig. 10), and finally

$$\log P_{\text{AGN}} [\text{years}] \approx 0.83 \log \frac{L_{\text{max}}}{L_{\text{min}}} + 1.15 \log \frac{M}{10^8 M_\odot} + 2.1 \quad (34)$$

for Active Galaxies (see fit on Fig. 11).

From the formula (31) we can estimate the values of masses of objects, if the values of P and A are known. The period-amplitude dependence is universal, and, in the coarse approximation, does not depend on μ . The positive correlation between period and amplitude indicates that those observables originate in a one nonlinear process, operating in a single timescale. Although the variability patterns can vary for different accretion rates, for a given mass the period and amplitude are strongly correlated and can describe the range of instability development. It can be in general adjusted by the specific model parameters, but the basic disk variability pattern is universal in that picture.

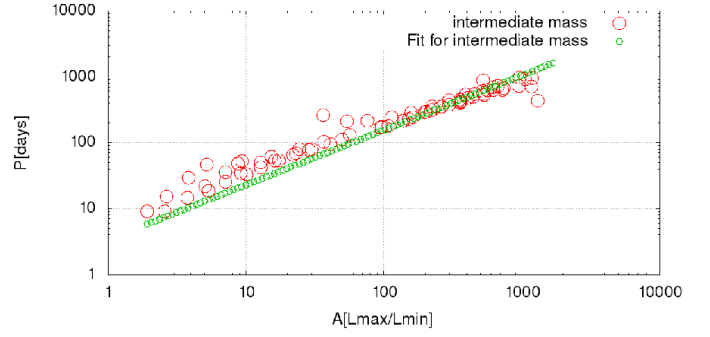


Fig. 10. Dependence between period and amplitude of outbursts for an intermediate mass black hole ($M = 3 \times 10^4 M_\odot$). The graph was prepared for a range of $\mu \in [0.44 : 0.8]$.

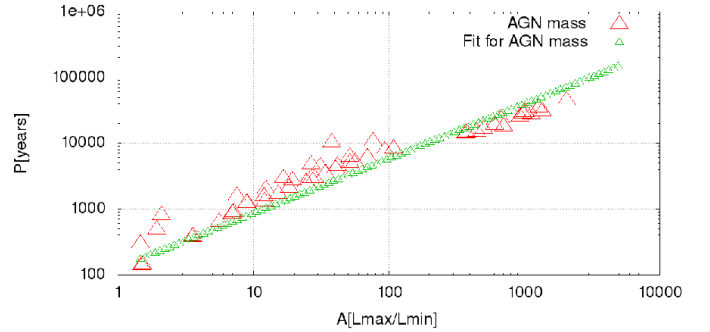


Fig. 11. Dependence between period and amplitude of outbursts for a supermassive black hole ($M = 10^8 M_\odot$). The graph was prepared for a range of $\mu \in [0.44 : 0.56]$.

5.4. Amplitude and width

In Figures 12, 13, and 14 the relation between the flare amplitude and its width is presented. Both values are dimensionless and show similar reciprocal behaviour for the black hole accretion disks outbursts across many orders of magnitude. The value of Δ can help us to distinguish between different states of the source. It should be also noticed, that Δ depends on the amplitude of the outburst only for small amplitudes, while for the larger ones, Δ remains approximately constant. The most convenient classification is to introduce the 'flickering' mode ($\Delta < 50$), which corresponds to the large ratio of the flare duration to its period ($\Delta > 0.15$), and the 'outburst' mode ($\Delta > 50$), which corresponds to the small flare duration to period ratio ($\Delta < 0.15$). The latter appears for high μ and \dot{m} , while the former occurs for low μ and \dot{m} .

5.5. Width, period and μ

In Figures 15, 16, and 17, the relation between the outbursts' period and their width is presented. The timescale of outbursts scales is approximately inversely proportional to the mass. According to the Figures 15, 16 and 17, the flare duration to period rate Δ depends on the value of accretion rate only weakly. The dependence on μ is more significant for all the probed masses. Thus, the outburst shape is determined mostly by the micro-physics of the turbulent flow and its magnetization, which is hidden in the μ parameter, and not by the amount of inflowing matter expressed by the value of accretion rate \dot{m} . In Figure 18, we present the result from Figs. 15, 16 and 17 with straight line fits connecting the values of Δ , μ , and the black hole mass M ,

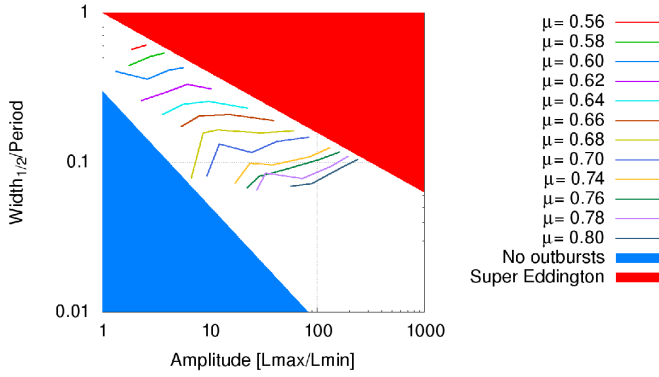


Fig. 12. Dependence between the amplitude and width of outbursts for stellar mass black hole ($M = 10M_{\odot}$). The graph was prepared for a range of $\mu \in [0.44 : 0.8]$. The color lines represent isolines for different μ

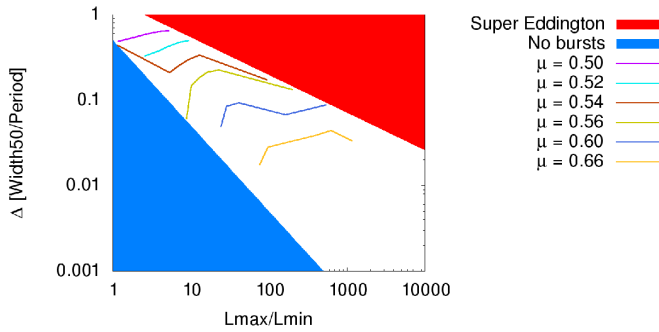


Fig. 13. Dependence between amplitude and width of outbursts for intermediate mass black hole ($M = 3 \times 10^4 M_{\odot}$). The graph was prepared for a range of $\mu \in [0.44 : 0.8]$. The color lines represent isolines for different μ

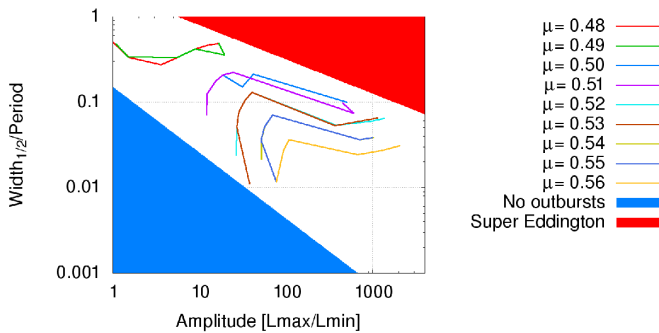


Fig. 14. Dependence between amplitude and width of outbursts for supermassive black hole ($M = 10^8 M_{\odot}$). The graph was prepared for a range of $\mu \in [0.44 : 0.56]$. The color lines represent isolines for different μ

which can be described by the formula:

$$-\log \Delta = (1.9 + 1.2 \log M)(\mu - 3/7). \quad (35)$$

From Eq. (35), we can conclude that the outburst shape depends predominantly on the disk magnetization. As a result, for larger μ we get in general narrower flares. This effect is even more pronounced for larger black hole masses. Therefore, the outburst flares occur more likely for larger values of μ .

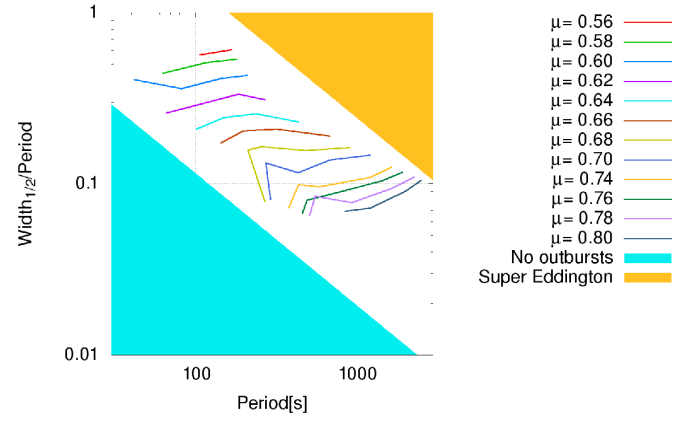


Fig. 15. Dependence between period and width of outbursts for stellar mass black hole ($M = 10M_{\odot}$). The graph was prepared for a range of $\mu \in [0.44 : 0.8]$. The color lines represent isolines for different μ

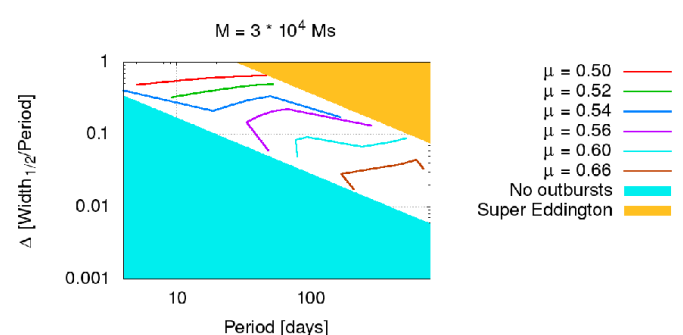


Fig. 16. Dependence between period and width of outbursts for intermediate mass black hole ($M = 3 \times 10^4 M_{\odot}$). The graph was prepared for a range of $\mu \in [0.44 : 0.8]$. The color lines represent isolines for different μ

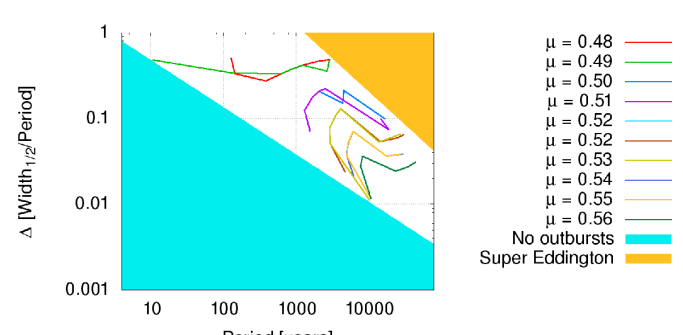


Fig. 17. Dependence between period and width of outbursts for supermassive black hole ($M = 10^8 M_{\odot}$). The graph was prepared for a range of $\mu \in [0.44 : 0.56]$. The color lines represent isolines for different μ

5.6. Amplitude and accretion rate

In the Figures 19, 20, and 21 we show the dependence between relative amplitudes and accretion rates \dot{m} for the stellar mass, intermediate mass and supermassive black holes, respectively. We see the monotonous dependence for any value of μ and mass. Because of the nonlinearity of evolution equations with respect of \dot{m} , we cannot present any simple scaling relation between \dot{m} and amplitudes nor periods.

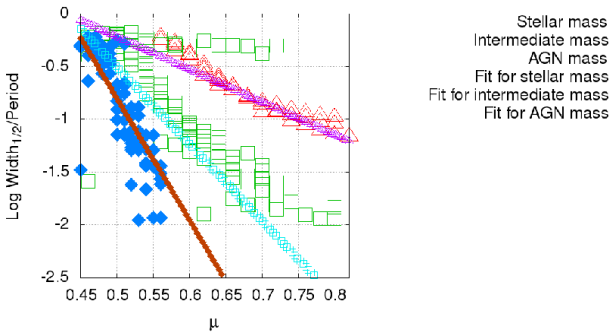


Fig. 18. Dependence between width, μ parameter and mass. One triangle represent one model. Triangles represent model for the stellar mass black hole accretion disks ($M = 10M_{\odot}$), squares represent model for the intermediate mass black hole accretion disks ($M = 3 \times 10^4 M_{\odot}$) and diamonds - model for the supermassive black hole accretion disks ($M = 3 \times 10^8 M_{\odot}$). Lines represent fits for each mass

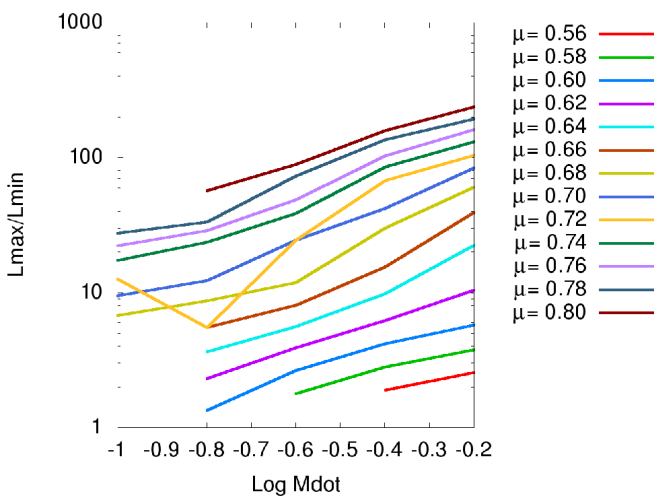


Fig. 19. Dependence between amplitude and accretion rate for stellar mass black hole ($M = 10M_{\odot}$). The graph was prepared for a range of μ . We can see simple unambiguous dependence for different μ -models

5.7. Limitations for the outburst amplitudes and periods

In Figures 12 and 15 the dark areas mark our numerical estimations for the possibly forbidden zones in the case of microquasar accretion disks. From those figures, we get the following fitting formulae:

$$0.3 \times A^{-0.77} < \Delta < A^{-0.4} \quad (36)$$

$$4 \times (P [s])^{-0.77} < \Delta < 50 \times P [s]^{-0.77}. \quad (37)$$

Eqs. (36) and (37) give in result the estimation for P and A

$$108 \times A^{0.516} < P [s] < 161 \times A^{1.4}. \quad (38)$$

In Figures 13 and 16 we have shown the estimated range of the possibly forbidden zones in the case of the accretion disks around the intermediate mass black holes. From those figures, we can derive the following formulae:

$$0.5 \times A^{-1} < \Delta < 1.5 \times A^{-0.44} \quad (39)$$

$$(P [\text{days}])^{-0.77} < \Delta < 13 \times P [\text{days}]^{-0.77}. \quad (40)$$

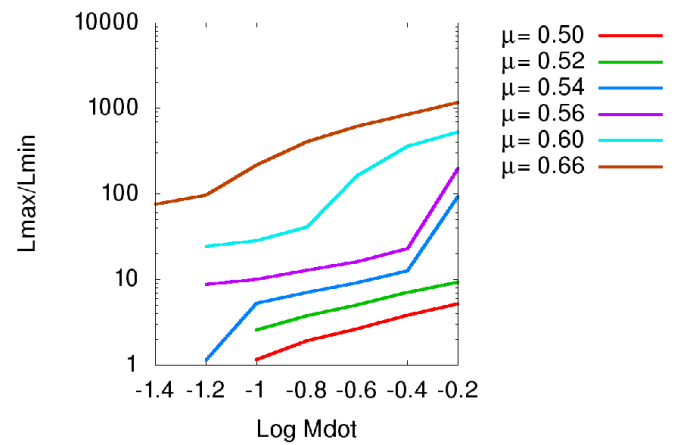


Fig. 20. Dependence between amplitude and accretion rate for an intermediate mass black hole ($M = 3 \times 10^4 M_{\odot}$). The graph was prepared for a range of μ . We can see simple unambiguous dependence for different μ -models

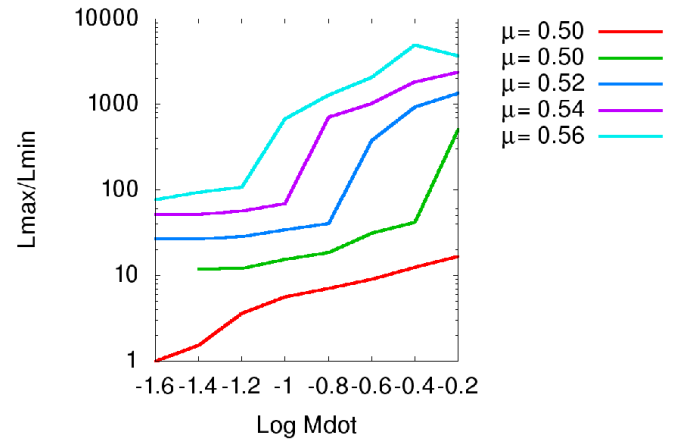


Fig. 21. Dependence between amplitude and accretion rate for a supermassive black hole ($M = 10^8 M_{\odot}$). The graph was prepared for a range of μ . We can see simple unambiguous dependence for different μ -models

Eqs. (39) and (40) give in result the estimation for P and A :

$$4.67 \times A^{0.568} < P < 16.6 \times A^{1.29}. \quad (41)$$

In figures 14 and 17 the dark shaded areas mark our estimations for the possibly forbidden zones for the case of supermassive black hole accretion disks. We get from those figures following formulae:

$$0.15 \times A^{-0.77} < \Delta < 2 \times A^{-0.4} \quad (42)$$

$$1.7 \times (P [\text{years}])^{-0.55} < \Delta < 250 \times (P [\text{years}])^{-0.77}. \quad (43)$$

Eqs. (42) and (43) give in result the estimation for P and A :

$$4.67 \times A^{0.568} < P < 16.6 \times A^{1.29}. \quad (44)$$

6. HLX-1 mass determination

The grids of models deliver some information about the correlation between the observed lightcurve features and the model

parameters. From the Eq. (31) we can determine the mass of object directly from its lighcurve:

$$M[M_\odot] = 0.45P[s]^{0.87}A^{-0.72} \quad (45)$$

The $\Delta - \mu - M$ dependence from Fig 18 and Eq. (35), combined with Eq. (45) gives us the exact estimation on μ

$$\mu = 3/7 + \frac{-\log \Delta}{1.49 + 1.04 \log P - 0.864 \log A}. \quad (46)$$

The ultraluminous X-ray sources (ULXs) are extragalactic X-ray sources that exceed the Eddington limit for accretion on stellar mass black hole (for $M = 10M_\odot$ the limit reaches 1.26×10^{39} erg/s). It is thought that those objects consist of black holes with masses at the level of $100 - 10^6 M_\odot$. Those objects are not the product of collapse of single massive stars (Davis et al. 2011). HLX-1 is the best known case of ULX, which has undergone six outbursts spread in the time over several years with an average period of about 400 days, duration time about 30-60 days, and ratio between its maximum and minimum luminosity L_{\max}/L_{\min} of about several tens. The exact average bolometric luminosity, computed from the SWIFT XRT observation is at the level of 3.22×10^{42} erg/s which gives the exact estimation for the mass from below $M > 2.4 \times 10^4 M_\odot$ (Wu et al. 2016, in. prep.) , since if the mass were less than $2.4 \times 10^4 M_\odot$ the accretion would be Super-Eddingtonian. The observed values of the source variability period, $P \approx 400$ days, and amplitude $A \approx 20$, and $\Delta \approx 0.13$, used in the Eqs. (45) and (46), result in the black hole mass of $M_{\text{BH,HLX-1}} \approx 1.9 \times 10^5 M_\odot$ and $\mu \approx 0.54$. Those values are close to the model parameters which are necessary to reproduce the lightcurve. Therefore, we conclude that our model of accretion disk with the modified viscosity law gives a proper explanation of HLX-1 outbursts. The model to data comparison, being the result of our analysis, is presented in the Figure 22.

7. Disk flare estimations

By computing a large grid of models we drive the general estimations for the oscillation period P , its amplitude A and relative duration Δ , despite the uncertainty of the viscosity parameter μ . The result are presented in Table 3.

We compare the allowed parameters of duration to period ratios (columns 3 and 4), periods (columns 5 and 6) and flare durations (columns 7 and 8). We get three values of relative amplitude for each source to present possible limitations for periods and duration times. The amplitude $A = 2$ represents faint outbursts, or flares, like those in the microquasar IGR J17091 (Janiuk et al. 2015). The amplitude $A = 10$ corresponds to a more developed instability case, like this in the ρ states of object GRS1915 (Belloni et al. 2000). The amplitude $A = 100$ is connected with the huge bursts, as in HLX-1 presented in the Figure 22. The timescales presented in the Tables are on the order of minutes for the microquasars, of months for the HLXs, and of millenia for the AGNs, which correspond to their viscous timescale. The period is strongly dependent on the amplitude and can change by several orders of magnitude for each mass. The estimations given here were made for the values of μ which are sufficient for the outbursts, but do not determine exactly the value of this parameter. Figure 23 (see next Section) presents a universal dependence between duration times and bolometric luminosities for the X-ray sources of different scales (microquasars with $M = 10M_\odot$, ULXs with $M = 3 \times 10^4 M_\odot$, and AGNs with $M = 10^8 M_\odot$). Exact duration values from the fit presented

in Eq. (48) are shown in the Table 4. For microquasars, the values included in the Table 3 corresponds to the typical values for small and intermediate flares, the same for the case of ULX. In case of AGN, the appearance of big flares is necessary to verify our model with the observational data presented in the Figure 23.

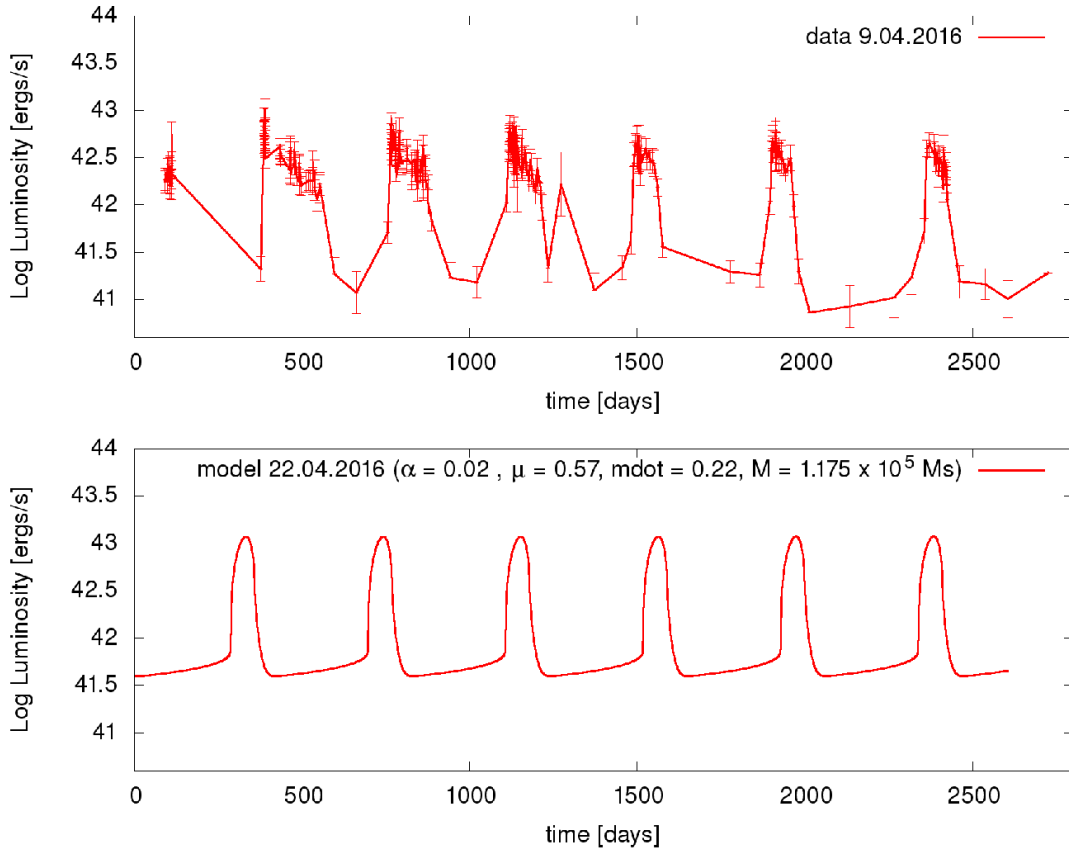


Fig. 22. Comparison between the SWIFT XRT observational lightcurve of HLX-1 (top panel) and the model (bottom panel). Model parameters: $\mu = 0.57$, $\alpha = 0.02$, $\dot{m} = 0.22$ and $M = 1.175 \times 10^5 M_\odot$

| Flare characteristic quantities for microquasars: | | | | | | | |
|--|-----|----------------|----------------|-------------------|-------------------|-------------------------|-------------------------|
| regime | A | lower Δ | upper Δ | lower P [s] | upper P [s] | lower $P\Delta$ [s] | upper $P\Delta$ [s] |
| small flicker | 2 | 0.176 | 0.758 | 154.43 | 425 | 27.17 | 322.15 |
| intermediate | 10 | 0.0509 | 0.398 | 354.34 | 4044 | 18.035 | 1610 |
| burst | 100 | 0.0086 | 0.158 | 1163 | 101580 | 10 | 16050 |
| Flare characteristic quantities for intermediate mass black holes: | | | | | | | |
| regime | A | lower Δ | upper Δ | lower P [days] | upper P [days] | lower $P\Delta$ [days] | upper $P\Delta$ [days] |
| small flicker | 2 | 0.25 | 1 | 7.056 | 40.6 | 1.756 | 40.6 |
| intermediate | 10 | 0.05 | 0.544 | 17.6 | 324 | 0.86 | 176.26 |
| burst | 100 | 0.005 | 0.198 | 65.1 | 6311 | 0.3255 | 1250 |
| Flare characteristic quantities for AGN: | | | | | | | |
| regime | A | lower Δ | upper Δ | lower P [years] | upper P [years] | lower $P\Delta$ [years] | upper $P\Delta$ [years] |
| small flicker | 2 | 0.088 | 1 | 114 | 209 | 100 | 209 |
| intermediate | 10 | 0.025 | 0.796 | 261.5 | 1956 | 65.4 | 1556 |
| burst | 100 | 0.00432 | 0.317 | 47662 | 320000 | 2059 | 101440 |

Table 3. Outburst duration values for three kinds of sources. The values for microquasars are expressed in seconds, values for ULXs in days and values for AGNs in years

| Source | Mass [M_\odot] | Duration for $L = 0.1L_{\text{Edd}}$ | Duration for $L = L_{\text{Edd}}$ |
|-------------|--------------------|--------------------------------------|-----------------------------------|
| Microquasar | 10 | 33 s | 595 s |
| ULX | 3×10^4 | 8.59 days | 153 days |
| AGN | 10^8 | 596 years | 10603 years |

Table 4. Outburst duration values for three kinds of sources. The values are taken from the Eq. (48)

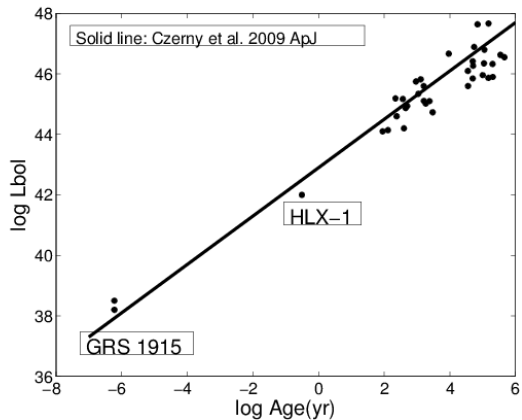


Fig. 23. Duration times and bolometric luminosities for the sources with accretion disks in different scales. Upper right corner correspond to the AGN. Lower left corner corresponds to microquasar, centre corresponds to IMBHs. The line represents the fit from Eq. (48).

8. Summary and discussion

In this work, we studied the accretion disk instability induced by the dominant radiation pressure, with the use of the generalized prescription for the stress tensor. We adopted a power-law dependence, with an index μ , to describe the contribution of the radiation pressure to the heat production. In other words, the strength of the radiation pressure instability deepens with the growing μ .

We computed a large grid of time-dependent models of accretion disks, parameterized by the black hole mass, and mass accretion rate. We used the values of these parameters which are characteristic for the microquasars, intermediate black holes, or AGN. One of our key findings is that this model can be directly applicable for determination of the black hole mass and accretion rate values, e.g., for the Ultraluminous X-ray source HLX-1, and possibly also for other sources.

We also found that the critical accretion rate, for which the thermal instability appears, decreases with the growing μ (see Figures 6,7,8). Also, the amplitudes of the outbursts of accretion disks in AGN are larger than the amplitudes of outbursts in microquasars and in IMBHs. The flare period grows monotonously with its amplitude, for any value of mass (see Figures 9, 10, 11). The outburst width remains in a well-defined relationship with its amplitude (see Figures 12,13,14).

We also found that there is a significant negative correlation between μ and the ratio of the flare duration to the variability period, Δ . On the other hand, the dependence between the outburst amplitude A and the mass accretion rate \dot{m} is non-linear and complicated.

Our results present different variability modes (Figures 4 and 5). The flickering mode is presented in Fig. 4. In this mode the relative amplitude is small, and flares repeats after one another. In the burst mode the amplitude is large, the maximum luminosity can be hundreds times greater than minimal. Exemplary lightcurve is shown in Fig. 5. In this mode we observe long separation between the flares (i.e. extended low luminosity state), dominated by the diffusive phenomena. Slow rise of the luminosity is the characteristic property of the disk instability model.

| source | ID | State | P | A | Δ | $M (M_\odot)$ | μ |
|--------|-------------|--------|----------|-----|----------|--------------------|-------|
| IGR | ν_I | ν | 45s | 2.5 | 0.15 | 6.38 | 0.717 |
| IGR | ρ_{IA} | ρ | 30s | 3.5 | 0.3 | 3.52 | 0.634 |
| IGR | ρ_{IB} | ρ | 30s | 4 | 0.4 | 3.198 | 0.589 |
| GRS | ν_G | ν | 90s | 4 | 0.1 | 8.31 | 0.763 |
| GRS | ρ_{GA} | ρ | 45s | 5 | 0.25 | 3.87 | 0.661 |
| GRS | ρ_{GB} | ρ | 40s | 4.5 | 0.4 | 3.77 | 0.583 |
| HLX | - | - | 400d | 2.5 | 0.14 | 1.88×10^5 | 0.534 |
| AGN | - | - | 10^5 y | 100 | 0.1 | 1.6×10^8 | 0.515 |

Table 5. Characteristic quantities of the RXTE PCA lightcurves for Galactic sources presented in (Altamirano et al. 2011b) (columns 4, 5, 6) supplemented with HLX and AGN, and estimations of the masses and magnetizations of sources (columns 7, 8). **Notation:** IGR = IGR J17091, GRS = GRS1915, HLX = HLX-1, AGN - typical value for the sample of AGNs presented in (Czerny et al. 2009). The OB-SIDs of the lightcurves are following: $\nu_I = 96420 - 01 - 05 - 00$, $\rho_{IA} = 96420 - 01 - 06 - 00$, $\rho_{IB} = 96420 - 01 - 07 - 00$, $\nu_G = 10408 - 01 - 40 - 00$, $\rho_{GA} = 20402 - 01 - 34 - 00$ and $\rho_{GB} = 93791 - 01 - 02 - 00$.

8.1. Radiation pressure instability in microquasars

Quantitatively, our numerical computations, as well as the fitting formula 31, give the adequate description of the characteristic 'heartbeat' oscillations of the two known microquasars: GRS 1915+105, and IGR 17091-324. Their profiles resemble those observed in the so-called ρ state of these sources, as found e.g. on 27th May, 1997 (Pahari et al. 2014).

For the microquasar IGR J17091, the period of the observed variability is less than 50s, as observed in the most regular heartbeat cases, i.e., in the ρ and μ states (Altamirano et al. 2011a). The ρ state is sometimes described as 'extremely regular' (Belloni et al. 2000), with period about 60–120 seconds for the case of GRS1915. The class μ includes typical Quasi-Periodic Oscillations with relative amplitude large than 2 and period 10–100s.

We apply the results of the current work to model the heartbeat states qualitatively.

Eqs. (31) and (35) allow us to determine the values of BH masses for the accretion disks and the μ parameter. The results are given in Table 5. For the ρ -type lightcurves we can estimate the masses of IGR J17091-3624 at the level of $3.2 - 3.5 M_\odot$ and GRS 1915+105 at the level of $3.7 - 3.9 M_\odot$. $\mu = 0.58 - 0.63$ for the IGR J17091-3624 and $0.58 - 0.66$ for the GRS 1915 respectively. From the ν -type lightcurves we get significantly larger values of masses and μ .

Our model thus works properly for the periodic and regular oscillations which are produced in the accretion disk for a broad range of parameters, if only the instability appears. Irregular variability states α , β , λ and μ should be regarded as results of other physical processes. The explanation of class κ of the microquasar GRS 1915 variable state (Belloni et al. 2000) which presents modulated QPOs seems to be on the border of applicability.

In our current model we neglected the presence of the accretion disk corona. According to Merloni & Nayakshin (2006), power fraction f emitted by corona is given by following formula:

$$f = \sqrt{\alpha} \left(\frac{P}{P_{\text{gas}}} \right)^{1-\mu}. \quad (47)$$

For our model with $\alpha = 0.02$, the values of f is low, and $f = 0.141 \left(\frac{P}{P_{\text{gas}}} \right)^{1-\mu}$, which for the values of μ investigated in the paper fulfills the inequality of $0.0125 < f < 0.141$, if we assume threshold maximal value of the gas-to-total pressure rate

$\beta = \frac{P_{\text{gas}}}{P}$ from Eq. 20. According to the fact that the (*heartbeat*) states are strongly radiation pressure dominated and the coronal emission rate is lower for lower values of the μ parameter, which are more likely to reproduce the observational data, we can regard the coronal emission as negligible.

8.2. Disk instability in the supermassive black holes

In the scenario of radiation pressure instability, with a considerable supply of the accreting matter, the outbursts should repeat regularly every $10^4 - 10^6$ years (Czerny et al. 2009). From the grid of models performed in (Czerny et al. 2009), done for $\mu = 0.5$ ($\tau_{r\phi} = \alpha \sqrt{PP_{\text{gas}}}$) and $10^7 M_{\odot} < M < 3 \times 10^9$, they obtained the following formula expressing correlation between the duration time, α parameter and bolometric luminosity L_{bol} :

$$\log\left(\frac{T_{\text{dur}}}{\text{yr}}\right) \approx 1.25 \log\left(\frac{L}{\text{ergs}^{-1}}\right) + 0.38 \log\left(\frac{\alpha}{0.02}\right) + 1.25 \log K - 53.6 \quad (48)$$

which, for the special case $\alpha = 0.02$ and neglecting the bolometric correction, has the following form:

$$\log L_{\text{bol}} = 0.8 \log\left(\frac{T_{\text{dur}}}{\text{s}}\right) + 42.88, \quad (49)$$

The formula (49) found its confirmation also in observational data for different scales of BH masses, as presented in Fig. 23. It applies despite the assumption of $\mu = 0.5$ since the expected dependence on μ is weak. If we combine Eqs. (31) and (35), we get:

$$\log T_{\text{dur}} = (1.15 - (\mu - 3/7)) \log M + 0.83 \log A - \mu - 0.03 \quad (50)$$

From the Figs. 12, 13 and 14 we can suggest the approximate dependence

$$\log A = 0.4 \log M + \text{const} \quad (51)$$

since for the same model input parameters (e.g. $\log \dot{m} = -0.2$, $\alpha = 0.02$ and $\mu = 0.56$) the amplitude could be even hundred times larger for the case of AGNs than for microquasars. Combining Eqs. (50) and (51) and adopting the proportionality between the black hole mass and bolometric luminosity (from full prescription $L_{\text{bol}} = \eta \dot{m} M$) we get:

$$\log T_{\text{dur}} = (1.99 - 1.2\mu)(\log L - \log \eta - \log \dot{m}) + \text{const.} \quad (52)$$

Assuming that Eddington accretion rate and accretion efficiency is roughly independent for different BH masses, the proportionality coefficient in Eq. 48 changes from 1.25 to 1.99 - 1.2μ , i.e. 1.27 for $\mu = 0.6$. For most of the known Active Galactic Nuclei, except Low Luminosity AGNs, their luminosity in Eddington units is over 0.02 (McHardy et al. 2006), and the sources remain in their soft state so the radiation pressure instability model should apply. The weak sources claimed to be AGN, like NGC4395 and NGC4258 (Lasota et al. 1996; Filippenko & Ho 2003) are claimed to be in hard state, being not described accurately by the model of Shakura-Sunyaev accretion disk.

It should be possible to study the evolution of those sources statistically. Based on the known masses, accretion rates and timescales for AGNs, the luminosity distribution for the samples of AGN with similar masses or accretion rates can be acquired. That should allow us to reproduce an average lightcurve for a

range of masses and accretion rates for survey of the known Active Galactic Nuclei (Wu 2009). The averaged lightcurve for big ensemble of AGN will help us to provide expected luminosity distribution or luminosity-mass, luminosity-duration relations with the AGNs existing in the universe. However, large amplitude outbursts may complicate the study since the detection of the sources between the outbursts may be strongly biased as the sources become very dim. Existence of the likely value of $\mu \approx 0.6$, proven by comparison of Eqs. (48) and (52) could also help in mass determination for newly discovered objects.

Another interesting topic, which could be noticed are so-called Changing-Look-AGNs, like IC751 (Ricci et al. 2016). Although most of the AGNs have a variability timescale on the order of thousands of years, the shape of model lightcurves (sharp and rapid luminosity increase) can suggest that for some cases luminosity changes can be observed.

8.3. Conclusions

We propose a possible application of the modified viscosity model as a description of a regular variability pattern (*heartbeat* states) of black hole accretion disks for the microquasars, ULXs and the Active Galactic Nuclei. The model works for the optically thick, geometrically thin disk. The model determines the range and scale of the radiation pressure instability. The parameter μ , which describes viscosity, can reproduce a possibly stabilizing influence of the strong magnetic field in the accretion disk. Nonlinearity of the models causes appearance of different modes of the disk state (stable disk, flickering, outbursts). Thanks to computing a large grid of models we can present quantitative estimations for the variability periods and amplitudes, and our model lightcurves reproduce several different variability patterns. Also, many observables, i.e., L , P , A , Δ , can be used directly to determine the physical parameters, like α , μ , M , and \dot{m} . Finally, our model can be successfully applied to the mass and accretion rate determination for the intermediate black hole HLX-1. The prospects of further applications for the microquasars and Active Galactic Nuclei are promising.

Acknowledgments

We thank Petra Sukova for helpful discussions. This work was supported in part by the grant DEC-2012/05/E/ST9/03914 from the Polish National Science Center.

References

- Abramowicz, M. A., Czerny, B., Lasota, J. P., & Szuszkiewicz, E. 1988, ApJ, 332, 646
- Altamirano, D., Belloni, T., Linares, M., et al. 2011a, ApJ, 742, L17
- Altamirano, D., Linares, M., van der Klis, M., et al. 2011b, The Astronomer's Telegram, 3225, 1
- Belloni, T., Klein-Wolt, M., Méndez, M., van der Klis, M., & van Paradijs, J. 2000, A&A, 355, 271
- Brandt, W. N., Mathur, S., & Elvis, M. 1997, MNRAS, 285, L25
- Capitanio, F., Del Santo, M., Bozzo, E., et al. 2012, MNRAS, 422, 3130
- Capitanio, F., Giroletti, M., Molina, M., et al. 2009, ApJ, 690, 1621
- Czerny, B., Nikołajuk, M., Różańska, A., et al. 2003, A&A, 412, 317
- Czerny, B., Siemiginowska, A., Janiuk, A., Nikiel-Wroczyński, B., & Stawarz, Ł. 2009, ApJ, 698, 840
- Davis, S. W., Narayan, R., Zhu, Y., et al. 2011, ApJ, 734, 111
- Done, C. & Davis, S. W. 2008, ApJ, 683, 389
- Filippenko, A. V. & Ho, L. C. 2003, ApJ, 588, L13
- Foschini, L., Berton, M., Caccianiga, A., et al. 2015, A&A, 575, A13
- Hirose, S., Krolik, J. H., & Stone, J. M. 2006, ApJ, 640, 901
- Honma, F., Kato, S., & Matsumoto, R. 1991, PASJ, 43, 147
- Janiuk, A. & Czerny, B. 2005, MNRAS, 356, 205

Janiuk, A. & Czerny, B. 2011, MNRAS, 414, 2186
 Janiuk, A., Czerny, B., & Siemiginowska, A. 2002, The Astrophysical Journal, 576, 908
 Janiuk, A., Grzedzielski, M., Capitanio, F., & Bianchi, S. 2015, A&A, 574, A92
 Janiuk, A. & Misra, R. 2012, A&A, 540, A114
 Jiang, Y.-F., Stone, J. M., & Davis, S. W. 2013, ApJ, 778, 65
 Kunert-Bajraszewska, M. & Janiuk, A. 2011, ApJ, 736, 125
 Kuulkers, E., Lutovinov, A., Parmar, A., et al. 2003, The Astronomer's Telegram, 149, 1
 Lasota, J.-P., Abramowicz, M. A., Chen, X., et al. 1996, ApJ, 462, 142
 Lasota, J.-P., Alexander, T., Dubus, G., et al. 2011, ApJ, 735, 89
 Lightman, A. P. & Eardley, D. M. 1974, ApJ, 187, L1
 McHardy, I. M., Koerding, E., Knigge, C., Uttley, P., & Fender, R. P. 2006, Nature, 444, 730
 Merloni, A. & Nayakshin, S. 2006, MNRAS, 372, 728
 Mishra, B., Fragile, P. C., Johnson, L. C., & Klužniak, W. 2016, ArXiv e-prints
 Nayakshin, S., Rappaport, S., & Melia, F. 2000, ApJ, 535, 798
 Neilsen, J., Remillard, R. A., & Lee, J. C. 2011, ApJ, 737, 69
 Pahari, M., Yadav, J. S., & Bhattacharyya, S. 2014, ApJ, 783, 141
 Peterson, B. M., McHardy, I. M., Wilkes, B. J., et al. 2000, ApJ, 542, 161
 Revnivtsev, M., Gilfanov, M., Churazov, E., & Sunyaev, R. 2003, The Astronomer's Telegram, 150, 1
 Ricci, C., Bauer, F. E., Arevalo, P., et al. 2016, ApJ, 820, 5
 Sadowski, A. 2016, ArXiv e-prints
 Sakimoto, P. J. & Coroniti, F. V. 1981, ApJ, 247, 19
 Sakimoto, P. J. & Coroniti, F. V. 1989, ApJ, 342, 49
 Shakura, N. I. & Sunyaev, R. A. 1973, A&A, 24, 337
 Straub, O., Godet, O., Webb, N., Servillat, M., & Barret, D. 2014, A&A, 569, A116
 Suková, P., Grzedzielski, M., & Janiuk, A. 2016, A&A, 586, A143
 Svensson, R. & Zdziarski, A. A. 1994, ApJ, 436, 599
 Szuszkiewicz, E. 1990, MNRAS, 244, 377
 Taam, R. E., Chen, X., & Swank, J. H. 1997, ApJ, 485, L83
 Taam, R. E. & Lin, D. N. C. 1984, ApJ, 287, 761
 Watarai, K.-y. & Mineshige, S. 2003, ApJ, 596, 421
 Wiersema, K., Farrell, S. A., Webb, N. A., et al. 2010, ApJ, 721, L102
 Wu, Q. 2009, MNRAS, 398, 1905